# Experimental and Theroretical Evaluation of Double Slope Single Basin Solar Stills: Study of Heat and Mass Transfer

**Manoj Dubey**
Department of Mechanical Engineering,
Jaypee University of Engineering and Technology
A.B. Road
Guna-473226
Madhya Pradesh
India

**Dhananjay R. Mishra**
Department of Mechanical Engineering
Jaypee University of Engineering and Technology
A.B. Road
Guna-473226
Madhya Pradesh
India

*Experimental and theoretical analysis of the three single basin double slope solar stills with 15˚, 30˚ and 45˚ glass cover inclinations, are carried out at meteorological conditions of Raghogarh, Guna (Latitude: 24°39'N, Longitude: 77°19'E, India). The experiments are performed from 14th to 16th June 2017. Detailed energy and exergy analysis are carried out using theoretical model proposed by Kumar & Tiwari, based on regression analysis. It has been observed that the theoretical results obtained from evaluation have good agreement with the experimental results. Maximum fresh water is obtained from 15˚ inclined glass cover solar still (viz.4.66 litre of 14 h observation ) and contribution of 52% and 48% from east and west side of solar still respectively. At 15:00 h all the stills show maximum thermal efficiency viz. 23.69, 29.24 and 25.09% for 15˚, 30˚ and 45˚ cover inclinations respectively. It has been observed that maximum exergy is lost in basin followed by glass and water in all the double slope solar stills.*

***Keywords:*** *solar stills, mass transfer, exergy, heat transfer*

## 1. INTRODUCTION

Water is an essential commodity on the earth surface. Due to rapid industrialisation and population growth, demand of potable water is increasing day by day. Today high and medium desalination techniques are available for producing drinking water from contami–nated water but these techniques mostly depend on the electricity (viz. conventional source of energy). Solar desalination is one of the prominent and environmental friendly method which uses solar energy for producing potable water. Experimental evaluation of double slope solar still integrated with parabolic trough collector having 28.1% higher productivity over the conventional solar still have been reported by Fathy et al. [1]. N identical evacuated tubular collectors integrated double slope solar still and its performance on the basis of exergy based energy payback time, duration, life cycle conversion and production factor have been reported by Singh and Al-Helal [2]. Experimental and numerical investigations of single and double effect solar distiller unit are reported by Kalbasi et al. [3]. Comparative studies on the solar still performance using different phase change materials has been performed and repor–ted by Kabeel et al. [4]. Experimental evaluation of conventional single slope solar still and its performance augmented with the nano material have been reported by Madhu et al. [5]. Annual performance along with the cost analysis of passive double slope solar still loaded with $Al_2O_3$, $TiO_2$ and CuO nanoparticles has been reported by Sahota et al. [6]. Effect of cover cooling flash tactic at 5 minute interval on passive and active double slope solar stills (integrated with flat plate solar collector) having highest productivity of 6.38 l/m$^2$day at 1 cm of water depth using 3 mm thick iron glass and 7.80 l/m$^2$day (through cover cooling) have been repor–ted by Morad et al.[7]. A comparative study of single and double basin double slope solar still of 0.63 m$^2$ basin area have been reported by Rajaseenivasan et al. [8]. Effect of water depth on distillate output of single slope passive distiller unit have been reported by Tiwari and Tiwari [9], whereas effect of various water depth for double slope single basin solar still (DSSS) facing north south have been reported by Ealngo et al. [10]. Effects of coal and metal chips on the performance of passive distiller unit have been reported by Mishra and Tiwari [11]. Khoula et al. [12,13] have reported the theoretical and experimental analysis of an air comp–ressor coupled hybrid solar still using artificial neural network (ANN). A detailed energy and exergy analysis of conventional and earth integrated solar still using Dunkle, Clark, Kumar & Tiwari, Tsilingiris and modi–fied Spalding's mass transfer theory has been reported by Dumka and Mishra [14,15]. Effect of different absorbing material (viz. Black rubber met, black ink and black dye) on DSSS of 3 m$^2$ basin area have been reported by Akash et al. [16]. Kalidasa Murugavel et al. [17] have reported the effect of various water depths and heat storage materials for a 2.08 m × 0.84 m DSSS, facing north-south. They have concluded that the maxi–mum value of production rate, water temperature and glass temperature variation inversely proportional to the heat capacity. Dwivedi and Tiwari [18] have concluded that the double slope solar still gives higher yield in the

Received: September 2018, Accepted: November 2018
Correspondence to: Dr Dhananjay R.Mishra
Department of Mechanical Engineering, Jaypee University of Engineering and Technology, India
E-mail: drm30680@yahoo.com
**doi: 10.5937/fmet1901101D**

peak summer months, while single slope solar still gives higher yield in winter months but the overall annual yi–eld of single slope solar still were higher as compared to annual yield obtained from the double slope solar still. The daily thermal and exergy efficiency of double slope were recorded to be higher as compared with single slope solar still. Two DSSS with single basin and dou–ble basin made of glass have been fabricated by Elango and Kalidasa Murugavel [19]. It has been reported by them that DSSS with basin insulation and without basin insulation gives 17.38% and 8.12% higher distillate output respectively as compared to single slope solar still. A detail review of integration of fins, usage of energy storing materials and wick materials, mixing of nanoparticles, agitation effect, transparent cover coo–ling, integration of thermoelectric cooler, multi effect of solar still, preheating with water heater and photovoltaic thermal collector, refine the condensing cover, operating with heat pump and refrigeration and integration with waste heat recovery have been reported by Srithar and Rajaseenivasan [20]. Reviews on various techniques used to lower glass cover temperature [21], numerous means of enhancing heat transfer [22,23], influence of various parameters [24], and thermal performance and exergy analysis of solar stills [25] are reported by various researchers.

In this paper, experimental and theoretical evalu–ation of 15˚, 30˚ and 45˚ inclined single basin double slope solar still is reported.

## 2. EXPERIMENTAL DETAILS

Three DSSS are fabricated using handlap method with the help of FRP material having 2m×1m basin area, 0.05 m wall thickness and 15˚, 30˚ and 45˚ of glass cover inclination (0.04 m thick).

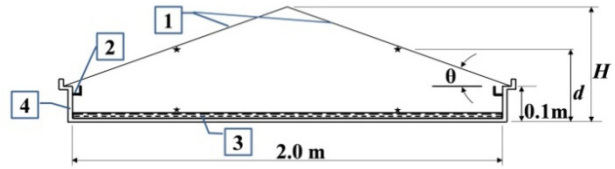


**Fig. 1(a). Schematic sectional diagram of DSSS 1-Glass cover, 2-Distillate collection channel, 3-Water, 4- FRP body, T-thermocouple, θ-Inclination of top cover from horizontal.**

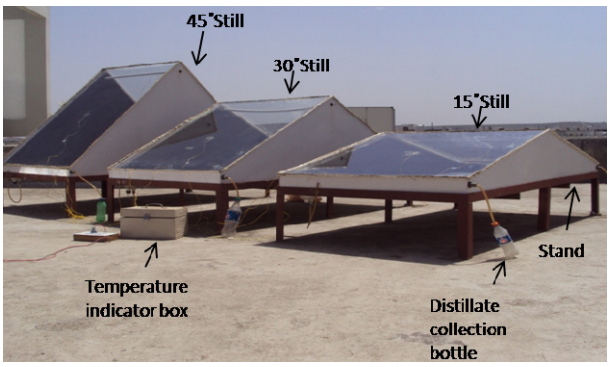


**Fig. 1(b): Actual photograph of experimental setup having 15˚, 30˚ and 45˚ surface inclination.**

Schematic and actual photograph of experimental setup are shown in Fig. 1(a) & (b) respectively. Solar stills are kept at same height and orientation (viz. east to west) Longer wall of solar stills are kept facing towards geographically south direction. Other constructional parameters of distiller units are tabulated in Table 1.

**Table 1. Dimensions of DSSSs having top cover inclination 15˚, 30˚ and 45˚ respectively.**

| Top cover inclination θ | 15˚ | 30˚ | 45˚ |
|---|---|---|---|
| Height of the still ***H*** (m) | 0.368 | 0.677 | 1.100 |
| Characteristic length d (m) | 0.234 | 0.388 | 0.600 |
| Area of top cover surface ($m^2$) | 2.0706 | 2.3094 | 2.8284 |

## 3. THEORITICAL BACKGROUND

The rate of heat transfer by convection from basin water to glass cover is described as:

$$\dot{q}_{cw} = h_{cw} \cdot \left(T_w - T_{ci}\right) \tag{1}$$

For the analysis of a convective heat transfer in the DSSS, Nusselt number (Nu), Grashof number (Gr), Prandtl number (Pr) and Rayleigh number (Ra) are need to be calculated.

$$N_u = \frac{h_{cw}}{\left(k/d\right)} = C\left(Gr \cdot Pr\right)^n \tag{2}$$

$$Gr = \frac{g \cdot \beta \cdot d^3 \cdot \rho \cdot \Delta T}{\mu^2} \tag{3}$$

$$Pr = \frac{\mu c_p}{k} \tag{4}$$

$$Ra = Gr \times Pr \tag{5}$$

For the evaluation of dimensionless numbers, mat–hematical relations for physical properties of water vapours reported by Toyama et al. [26]are used.

Based on different ranges of Gr number, many authors have proposed values of C and n. Semi-empi–rical formula for convective heat transfer coeffi–cient ($h_{cw}$) calculation, propose by Dunkle [27] is best suited for Gr > 3.2 ×$10^5$ and mean and operating temperature range of 50°C and 17 °C respectively. He used C as 0.075 and n as 1/3 which makes $h_{cw}$ inde–pendent of $d$. Convective heat transfer coefficient from water to glass surface can be calculated using the relation:

$$h_{cw} = 0.884\left[T_w - T_{ci} + \frac{\left(P_w - P_{ci}\right)\left(T_w + 273\right)}{2.689\times10^5 - P_w}\right]^{\frac{1}{3}} \tag{6}$$

Clark [28]simulated the solar radiation and wind flow steady state conditions in 1990. Based on his in–door experiment, he has proposed values of C and n based on the operating range more than 55 °C. He has observed that the value of $h_{cw}$ reduces by 1/2 in compa–rison to Dunkle model, because in ideal condition eva–poration and condensation rates remain same. The values of C and n proposed by Clark are as follows:

$$C = 0.21, n = \frac{1}{4}\ for 10^4 < Gr < 2.5\times10^5,$$

$$C = 0.1255, n = \frac{1}{4}\ for 2.51\times10^5 < Gr < 10^7$$

A thermal model based on linear regression has pro–posed by Kumar and Tiwari [29]. Experimental yield were used in this model to generate C and n values for the still. The model had an edge over other models that it did not have any limitation of Gr number. The relations for C and n from the model are as follows:

$$n = \frac{N\left(\sum x, y\right) - \left(\sum x\right)\cdot\left(\sum y\right)}{N\left(\sum x^2\right) - \left(\sum x\right)^2} \tag{7}$$

$$C = \exp\left(\frac{\sum y}{N} - n\frac{\sum x}{N}\right) \tag{8}$$

After calculating $h_{cw}$ using Equation (2), evaporative heat transfer coefficient ($h_{ew}$) can be calculated using following relation [30]:

$$h_{ew} = 0.016273.\ h_{cw}\left(\frac{P_w - P_{ci}}{T_w - T_{ci}}\right) \tag{9}$$

Then yield can be calculated as:

$$\dot{m}_{ew} = \frac{\dot{q}_{ew}\cdot A_s \cdot 3600}{L} = \frac{h_{ew}\cdot A_s \cdot \left(T_w - T_{ci}\right)\cdot 3600}{L} \tag{10}$$

Rate of radiative heat transfer from water to glass surface is calculated as [30]:

$$\dot{q}_{rw} = h_{rw}\cdot F_{12}\cdot\left[\left(T_w - T_{ci}\right)\right] \tag{11}$$

where,

$$h_{rw} = \varepsilon_{eff}\cdot\sigma\cdot\left[\left(T_w + 273.15\right)^2 + \left(T_{ci} + 273.15\right)^2\right] \tag{12}$$
$$\left[T_w + T_{ci} + 546.2\right]$$

$$\frac{1}{\varepsilon_{eff}} = \frac{1}{\varepsilon_w} + \frac{1}{\varepsilon_{ci}} - 1 \tag{13}$$

Total internal heat transfer coefficient from water to inner glass surface is given by:

$$h_{1w} = h_{cw} + h_{ew} + h_{rw} \tag{14}$$

Total heat transfer rate from water to inner glass surface is given by:

$$\dot{q}_1 = \dot{q}_{cw} + \dot{q}_{ew} + \dot{q}_{rw} \tag{15}$$

To predict the dominance of individual mode of heat transfer in DSSS, energy fractions are used. These are expressed as the ratio of heat transfer rate from a spe–cific mode to that of total heat transfer rate [30]. These energy fractions are described as follows:

$$F_{ew} = \frac{\dot{q}_{ew}}{\dot{q}_1};\ F_{cw} = \frac{\dot{q}_{cw}}{\dot{q}_1};\ F_{rw} = \frac{\dot{q}_{rw}}{\dot{q}_1} \tag{16}$$

The instantaneous thermal efficiency of solar still is described as [31]:

$$n_i = \frac{\dot{m}_{ew} L}{I(t)\, A_s} \tag{17}$$

Exergy efficiency is calculated as[32,33]:

$$\eta_{Ex} = \frac{\dot{E}x_{evap}}{\dot{E}x_{in}} \tag{18}$$

The exergy destruction for water, basin area and glass surface can be calculated as:

$$\dot{E}x_{dest,water} = \tau_g\alpha_w\dot{E}x_{in} + \dot{E}x_{water} - \tag{19}$$
$$-\dot{E}x_{trans(water\to glass)}$$

$$\dot{E}x_{dest,basin} = \tau_g\tau_w\alpha_w\dot{E}x_{in} - \left(\dot{E}x_{water} - \dot{E}x_{insu}\right) \tag{20}$$

$$\dot{E}x_{dest,water} = \alpha_w\dot{E}x_{in} + \dot{E}x_{trans(water\to glass)} - \tag{21}$$
$$-\dot{E}x_{water(glass\to airs)}$$

## 4. RESULTS AND DISCUSSION

Solar radiations on cover surface of the solar distiller units were recorded from 6:00 to 19:00 h during the experimentation, and their change with time is shown in Fig. 2. The maximum solar radiation on the east cover surfaces of 15˚, 30˚ and 45˚ was recorded 1141 W/m$^2$ at 11:00 h, 1128 W/m$^2$ at 10:30 h and 1120 W/m$^2$ at 10:00 h respectively. whereas minimum solar radiation on those surfaces were recorded as 22, 20 and 10 W/m$^2$ respectively, at 19:00 h. Similarly maximum solar radiation on the west cover surfaces of 15˚, 30˚ and 45˚ stills is recorded 1146 W/m$^2$ at 12:30 h, 1179 W/m$^2$ at 14 h and 1138 W/m$^2$ at respectively. Whereas the minimum solar radiation on those surfaces is recorded as 20, 22 and 22 W/m$^2$ respectively, at 19:00 h.

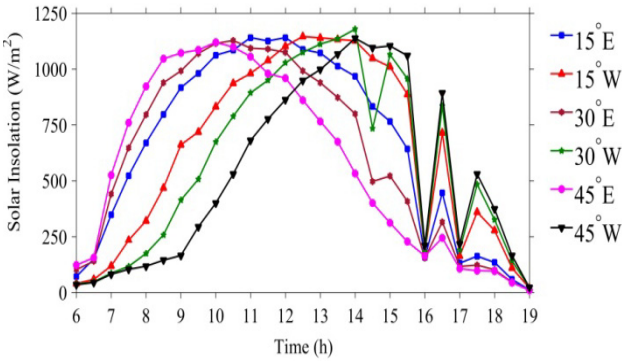


**Fig. 2. Change in solar radiation with time.**

It is evident that as the inclination of top cover dec–reases, time of maximum solar radiation, shifts towards the solar noon and thus the intensity of maximum solar radiation also increases. It is also observed that on east side top cover surface of DSSS, as the glass cover inclination increases, the time of peak insolation shifts towards morning, whereas on the west side top cover surface, the peak insolation shifts towards evening with increase in top cover inclination. A sudden fall in the insolation at 14:30 h, 16:00 h and 17:00 h is due to a temporary cloud. It is found that the slope of the solar radiation curve in forenoon, on east cover of 45˚ is steepest, and it decreases with decrease in cover inc–lination, from 6:00 h to 9:00 h, whereas in afternoon, from 16:00h to 19:00h, the slope of the curve is steepest for 15˚ and it decreases with increase in cover slope. The pattern reverses on west covers. In the forenoon,

the slope of solar radiation curve for 15˚ is steepest and it decreases with increase in cover inclination but in the afternoon, the curve for 45˚ is steepest and it reduces with reduction in cover inclination. These variations in solar radiations on the glass covers are due to geogra–phical location, tilt angles and surface azimuth angles.

Variation in basin water temperature ($T_w$), inner glass cover temperature ($T_{ci}$) and ambient temperature ($T_a$) in all DSSSs, for east side are shown in Fig. 3. and that for the west side are shown in Fig. 4.

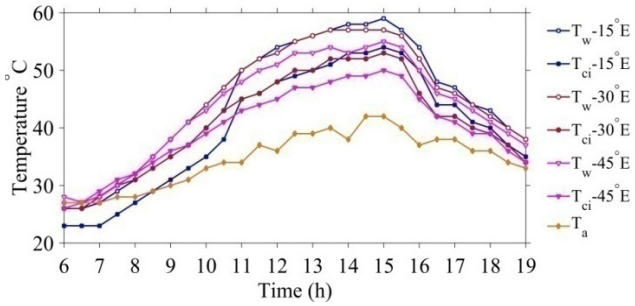


**Fig. 3. Variation of $T_w$ and $T_{ci}$ in east side of 15˚ 30˚ and 45˚ DSSS with time.**

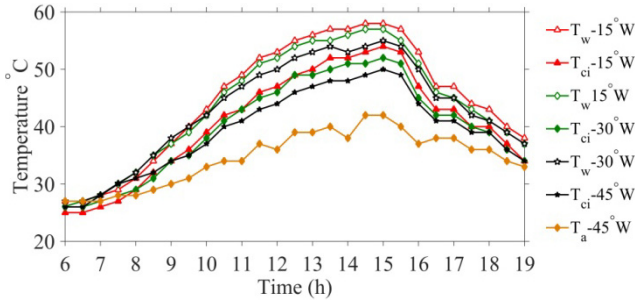


**Fig. 4. Variation of $T_w$ and $T_{ci}$ in west side of 15˚ 30˚ and 45˚ DSSS with time.**

Maximum 'condensing cover inner surface tempe–rature', $T_{ci}$, in east side of 15˚, 30˚ and 45˚ stills were recorded as 54˚C, 53˚C, and 50˚C respectively, at 15:00 h, whereas minimum $T_{ci}$, were recorded as 23˚, 26˚ and 26˚C respectively, at 6:00 h. Maximum $T_{ci}$, in east side of 15˚distiller unit was 8% higher than 45˚ distiller unit and was 1.8 % higher than 30˚ distiller unit whereas that in west side of 15˚ distiller unit was 8% higher than 45˚ distiller unit and was 3.8% higher than 30˚ distiller unit. Maximum $T_{ci}$ in west side of 15˚, 30˚ and 45˚ stills were recorded as 54˚C, 52˚C and 50˚C respectively, at 15:00 h respectively, whereas minimum $T_{ci}$, were recorded as 25˚, 26˚ and 26˚C respectively, at 6:00 h. The maximum 'basin water temperature', $T_w$, in east side of 15˚, 30˚ and 45˚ stills were recorded as 59˚C respectively. Maxi–mum $T_w$ in east side of 15˚ still was 7.2% higher than 45˚ still and was 3.5 % higher than 30˚ still whereas that in west side of 15˚ still was 5.4% higher than 45˚ still and was 1.75% higher than 30˚ still. Maximum $T_w$, in west side of 15˚, 30˚ and 45˚ distiller units were recorded as 58˚C at 14:30 h, 57˚C at 14:30 h and 55˚C at 15:00 h respectively, whereas minimum were re–corded as 27˚, 26˚ and 26˚C respectively, at 6:00 h. The minimum and maximum values of ($T_w$ - $T_{ci}$ ) in east side of 15˚, 30˚ and 45˚ DSSS were recorded as 3 and 6, 0 and 6, -1 and 6˚C at 6:00 and 11:30, 7:00 and 11:30, 7:00 and 11:30 h respectively, whereas that in west side of 15˚, 30˚ and 45˚ DSSS were recorded as 2 and 6, 0 and 6, 0 and 6˚C at 6:00 and 11:00, 6:00 and 11:30, 7:00 and 11:00 h respectively. On comparing $T_w$ and $T_{ci}$ in the east sides of 15˚, 30˚ and 45˚ DSSSs, it was observed that initially both had lowest value in 15˚ still, but at 11:00 it took over to 30˚ and 45˚ DSSSs and then remained higher till 19:00 h. The peak temperatures in 15˚, 30˚ and 45˚ DSSS were found to be in decreasing order. This is due to the still geometry viz. Glass cover inclination and characteristic length. The pattern of temperature rise and fall of $T_w$ and $T_{ci}$ were found to be reversed in the west sides of 15˚, 30˚ and 45˚ DSSS.

Variation in partial pressure at water surface and inner condensing cover with time is shown in Fig. 5 and Fig. 6.

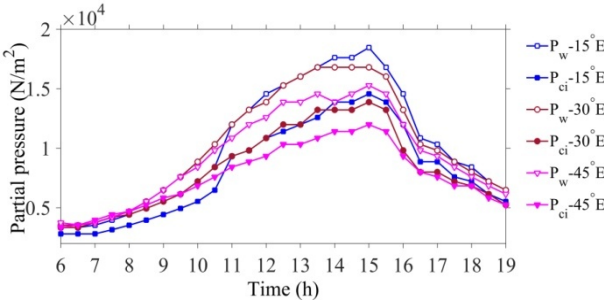


**Fig. 5. Variation of $P_w$ and $P_{ci}$ in east side of 15˚ 30˚ and 45˚ DSSS with time.**

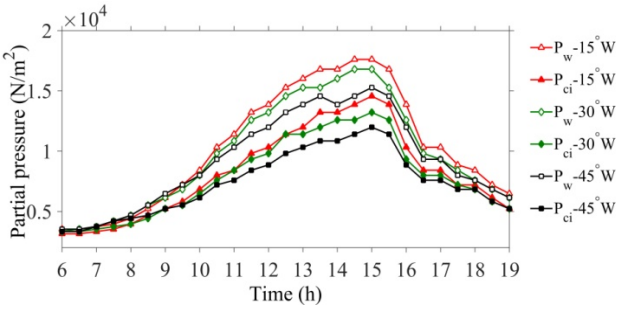


**Fig. 6. Variation of $P_w$ and $P_{ci}$ in west side of 15˚ 30˚ and 45˚ DSSS with respect to time.**

Partial pressure is function of temperature and therefore the nature of variation of $P_w$ and $P_{ci}$ are similar to that of $T_w$ and $T_{ci}$. Partial pressures may be evaluated using relations given by Toyama et al. [26]. In the east side of 15˚ still, $P_w$ was observed to be 3337.53 N/m$^2$ at 6:00 h, attains a highest value of 18453.77 N/m$^2$ at 15:00 h and drops down to 6482.15 N/m$^2$ at 19:00 h. The rate of increase of $P_w$ in forenoon session is lower than its rate of decrease in afternoon session in both east and west sides. Maximum value of $P_w$ , in east side of 15˚ 30˚ and 45˚still were observed as 18453.77, 16800 and 15276.53 N/m$^2$ respectively, whereas maxi–mum values of $P_{ci}$, in east side of 15˚ 30˚ and 45˚ still were observed as 14561.16 N/m$^2$, 13875.21 N/m$^2$ and 11983.71 N/m$^2$ respectively. Maximum value of $P_w$, in west side of 15˚ 30˚ and 45˚ still were observed as 17609.86 N/m$^2$, 16800 N/m$^2$ and 15276.53 N/m$^2$ res–pectively, whereas maximum values of $P_{ci}$, in west side of 15˚ 30˚ and 45˚still were observed as 14561.16, 13217.64 and 11983.71 N/m$^2$ respectively. In east side of distiller units, difference of $P_w$ and $P_{ci}$, was observed maximum 4212.32 N/m$^2$ in 15˚ DSSS at 13:30 h,

followed by 4038.67 N/m$^2$ in 30˚ DSSS at 13:00 h, followed by 3709.45 N/m$^2$ in 45˚ DSSS at 13:30 h. Whereas that ob–served in west side was maximum 4038.67 N/m$^2$, in 15˚ DSSS at 13:00 h, followed by 4212.32 N/m$^2$ in 30˚ DSSS at 14:30 h, followed by 3709.45 N/m$^2$ in 45˚ DSSS at 13:30 h. The maximum value of $P_w$ in east side of 15˚ still is 20.8% higher than 45˚ and 9.8% higher than 30˚ still whereas maximum value of $P_{ci}$ in east side of 15˚ still is 21.5% higher than 45˚ and 4.9% higher than 30˚ still. Similarly the maxi–mum value of $P_w$ in west side of 15˚ still is 15.3% hig–her than 45˚ still and 4.8% higher than 30˚ still whereas maximum value of $P_{ci}$ in east side of 15˚ still is 21.5% higher than 45˚ still and 10.1% higher than 30˚ still.

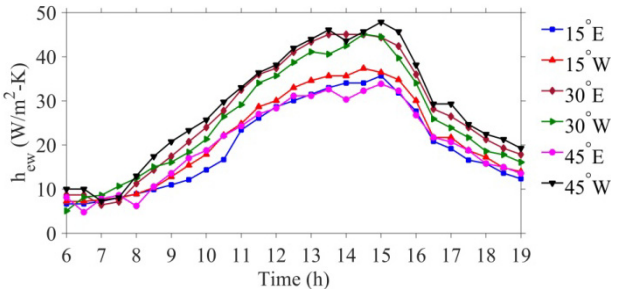


**Fig. 7. Variation of evaporative heat transfer coefficient from water to condensing cover inner surface with respect to time.**

'Evaporative heat transfer coefficient', $h_{ew}$, from water to inner surface of condensing cover is evaluated using Kumar & Tiwari model for 15˚, 30˚ and 45˚ stills and variation of $h_{ew}$ with time is plotted in Fig. 7. The maximum $h_{ew}$ from water to condensing cover surface on east side of 15˚, 30˚ and 45˚ stills is evaluated as 35.83 W/m$^2$-K at 15:00 h, 45.59 W/m$^2$ -K at 13:30 h and 33.06 W/m$^2$ –K at 15:00 h respectively, whereas minimum $h_{ew}$ in these distiller units was evaluated as 6.61 W/m$^2$ –K at 6:00 h, 6.14 W/m$^2$ -K at 7:00 h and 4.65 W/m$^2$ -K at 6.30 h respectively. The maximum $h_{ew}$ from water to condensing cover surface on west side of 15˚, 30˚ and 45˚ stills are evaluated as 37.56 W/m$^2$ -K at 14:30 h, 45.52 W/m$^2$ -K at 14:30 h and 47.85 W/m$^2$ -K at 15:00 h respectively, whereas minimum of that is evaluated as 7.13 W/m$^2$ -K at 14:30 h, 4.89 W/m$^2$ -K at 14:30 h and 7.31 W/m$^2$ -K at 15:00 h respectively. The maximum $h_{ew}$ on east side of 30˚ still is 27.2% higher than 15˚ still and 37.9% higher than 30˚ still, while The maximum value of $h_{ew}$ on west side of 45˚ still is 27.39% higher than 15˚ still and 5.11% higher than 30˚ still. It is also observed that in 15˚ and 30˚ stills the eva–porative heat transfer coefficient on east and west side exhibit the same pattern but in 45˚ still evaporative heat transfer coefficient on west side is 44.7% higher than that on east side.

'Convective heat transfer coefficient', $h_{cw}$, from water to inner surface of condensing cover is also eva–luated using Kumar & Tiwari model and its variation with time is plotted in Fig. 8.

Maximum value of $h_{cw}$ from basin water to inner surface of condensing cover in the east side of 15˚, 30˚ and 45˚ DSSS is evaluated as 2.90 W/m$^2$ -K at 13:30 h, 4.02 W/m$^2$ -K at 13:00 h and 3.17 W/m$^2$ -K at 13:30 h respectively, whereas minimum of that is evaluated as 2.28 W/m$^2$ -K at 6:00 h, 1.77 W/m$^2$ -K at 7:00 h and 1.41 W/m$^2$ -K at 6:30 h respectively. The maximum value of $h_{cw}$ from basin water to inner surface of con–densing cover in the west side of 15˚, 30˚ and 45˚ DSSS is evaluated as 3.18 W/m$^2$-K at 13:00 h, 3.98 W/m$^2$ -K at 14:30 h and 4.58 W/m$^2$-K at 13:30 h respectively, whereas minimum of that is evaluated as 2.28 W/m$^2$ –K at 6:00 h, 1.56 at 6:00 h and 1.56 W/m$^2$ –K at 7:00 h respectively. It is observed that for 15˚condensing cover inclination, $h_{cw}$ rises gradually with time but for con–densing cover inclination higher than 15˚, $h_{cw}$ initially drops then rises. On east side, average $h_{cw}$ for 30˚DSSS was 32.4 % higher than 15˚DSSS and 26.6 % higher than 45˚DSSS, whereas for west side, average $h_{cw}$ for 45˚ DSSS was 43.7 % higher than 15˚ and 17 % higher than 30˚ still.

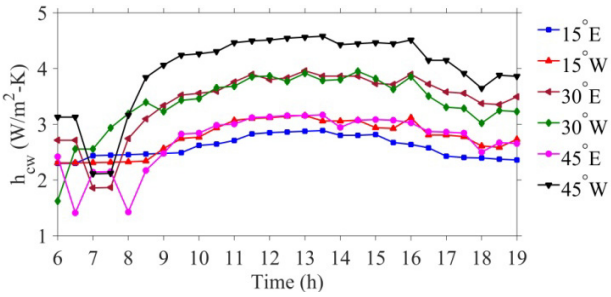


**Fig. 8. Variation of convective heat transfer coefficient from water to inner surface of condensing cover with time.**

Radiative heat transfer coefficient, $h_{rw}$, from basin water to inner surface of the condensing cover is evalu–ated using Kumar & Tiwari model and its variation with time is plotted in Fig. 9. The maximum value of $h_{rw}$ in the east side of 15˚, 30˚, and 45˚ distiller units is evaluated as 6.64 , 6.55 and 6.40 W/m$^2$ –K, at 15:00 h respectively, whereas minimum of that is evaluated as 4.89, 4.98 and 5.01 W/m$^2$ –K, at 6:00 h respectively. Similarly the maximum value of $h_{rw}$ in the west side of 15˚, 30˚ and 45˚ distiller units is evaluated as 6.61, 6.52 and 6.4 W/m$^2$ –K at 15:00 h respectively, whereas mini–mum of that is evaluated as 4.96, 4.96 and 4.98 W/m$^2$ –K, at 6:00 h respectively. It is quite evident from the data that the $h_{rw}$ does show marginal difference with respect to cover inclination or direction(i.e. east or west), but its value in 15˚ supersedes 30˚ and 45˚ stills at 11:00 h and remains higher till 19:00 h. Similarly its value for 30˚ still also supersedes 45˚ and remains higher till 19:00 h.

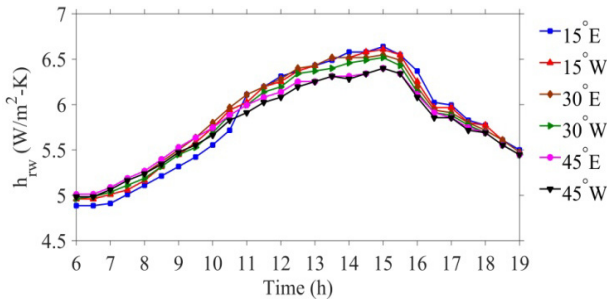


**Fig. 9. Variation in radiative heat transfer coefficient with time.**

Total heat transfer coefficient, $h_{1w}$, from basin water to inner surface of condensing cover is calculated using Kumar & Tiwari model and its variation with time is plotted in Fig. 10. Maximum value of $h_{1w}$ in east side of

15˚, 30˚ and 45˚ distiller units is evaluated as 45.3 W/m$^2$ –K at 15:00 h, 56.02 W/m$^2$ –K at 14:30 h and 42.55 W/m$^2$ –K at 15:00 h respectively, whereas minimum of that is evaluated as 13.78 W/m$^2$ –K at 6:00 h, 12.97 W/m$^2$ –K at 7:00 h and 11.07 W/m$^2$ –K at 6:30 h respectively. Similarly maximum $h_{1w}$ in west side of 15˚, 30˚ and 45˚ distiller units is evaluated as 47.23 W/m$^2$ –K at 14:30 h, 56 W/m$^2$ –K at 14:30 h and 58.72 W/m$^2$ –K at 15:00 h respectively, whereas minimum of that is evaluated as 14.37 W/m$^2$ –K at 6:00 h, 11.42 W/m$^2$ –K at 6:00 h and 14.49 W/m$^2$ –K at 7:00 h respectively. It is observed that in east side $h_{1w}$ was highest in 30˚ still which is 29.4% higher than 15˚ still and 28.4% higher than 45˚ still whereas in west side the highest average $h_{1w}$ was in 45˚still which is 26.1% higher than 15˚ still and 9.8% higher than 30˚ still. The value of $h_{1w}$ rises from 6:00 h to 15:00 h and then falls down from15:00 h to 19:00 h so the slope of the curve is less during 6:00 h to 15:00 h.

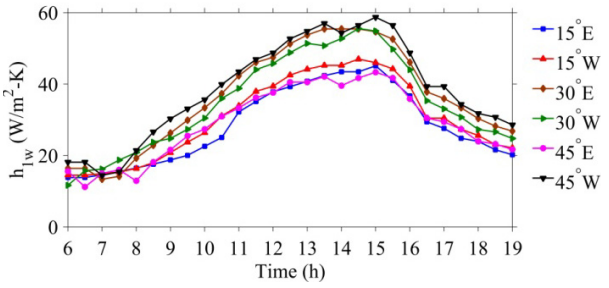


**Fig. 10. Variation in total heat transfer coefficient from basin water to inner surface of condensing cover with respect to time.**

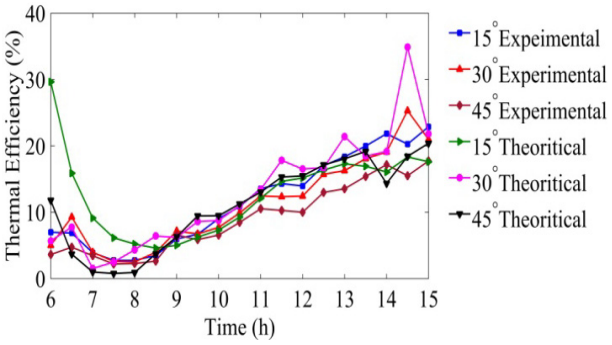


**Fig. 11. Variation of theoretical and experimental instanta–neous thermal efficiency with respect to time.**

The theoretical and experimental instantaneous exe–rgy efficiencies, $\eta_i$, were calculated for all the DSSSs using Eq.18 The change in efficiency with time, from 6:00h to 15:00h is shown in Fig. 11. The maximum value of experimental $\eta_i$ was 25.32%, at 14:30h, in the distiller unit with 30˚top cover inclination, which is 10.66% and 42.73% higher respectively in comparison to stills with top cover inclinations 15˚ and 45˚. Theo–retical $\eta_i$ was also calculated for all the distiller units. Its highest value, 34.9%, was also in distiller unit having 30˚ top cover inclination which is 17.63% and 71.1% higher in comparison to stills having cover inclinations 15˚and 45˚ respectively. However the average theo–retical $\eta_i$ was highest, in 15˚ still which is also validated by the experimental results. The experimental and theo–retical $\eta_i$ are in good agreement with each other, in the DSSS with 15˚ cover inclination. The variation between experimental and theoretical values of $\eta_i$ increases with increase in top cover inclination, which is due to devi–ation from basic assumptions of Kumar & Tiwari model. As the top cover inclination increases, the value of solar radiation also increases, especially in morning and evening hours, but the distance to be travelled by vapour from basin to condensing cover, also increase, thus predicted theoretical efficiencies are higher than experimental.

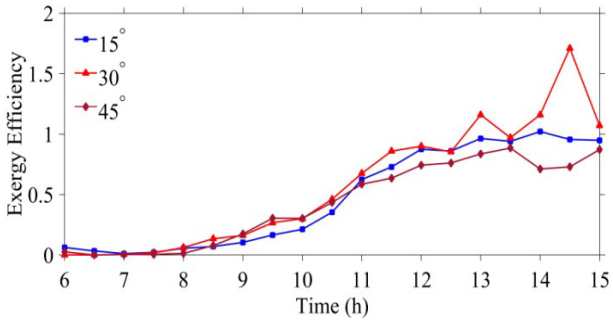


**Fig. 12. Exergy efficiency in percentage as a function of time.**

Exergy efficiency of all the DSSSs were evaluated using Kumar & Tiwari model and plotted with time in Fig. 12. Maximum exergy efficiency was recorded as 1.71% in DSSS having top cover inclination 30˚, at 2:30h, which is 67.64% and 94.31% higher in compa–rison to stills having top cover inclination of 15˚ and 45˚ respectively. Minimum exergy efficiency is zero in all the stills. The average exergy efficiency is also maxi–mum in the still with top cover inclination 30˚. Its value in 30˚ still is 0.57, which is 21.28% and 32.56% higher than stills having top cover inclination of 15˚ and 45˚ respectively.

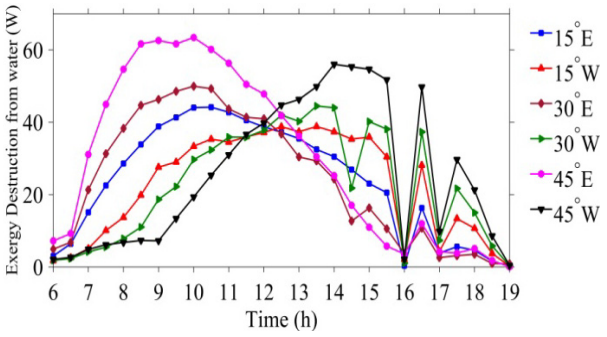


**Fig. 13. Variation in exergy destruction from basin water with time.**

Exergy destruction from basin water for 15˚, 30˚ and 45˚ DSSS has been evaluated using Kumar & Tiwari model and its variation is plotted with respect time in Fig. 13.

Exergy destruction from basin water in east side of distiller units in morning, noon and evening have been evaluated as 3.10, 42.55, 0 W in 15˚ at 6:00, 10:30, 19:00 h; 4.27, 42.72, 0 W in 30˚ at 6:00, 10:00, 19:00 h; 5.08, 44.11, 0 W in 45˚ at 6:00, 10:00, 19:00 h, whereas that in west side of distiller units have been evaluated as 1.68, 37.11, 0 W in 15˚ at 6:00, 13:30, 19:00 h; 1.59, 37.09, 0.17 W in 30˚ at 6:00 and 13:30 and 19:00; 1.47, 36.41, 0.02 W in 45˚ at 6:00, 14:30, 19:00 h.

The time of maximum exergy destruction, in east sides of distiller units, shifts towards morning hours with increase in cover inclination, while in west sides it shifts towards evening, with increase in cover inclination. In the east side of distiller units, the average slope of exergy destruction curves, in forenoon hours, is lowest for 15˚ and it increases with increase in cover inclination. In afternoon hours, during reduction in exergy destruction the average slope of exergy destruction curve is less in comparison to forenoon hours but the effect of change in slope remains same. But in west side of distiller units the average slope of exergy destruction curves, in forenoon hours, is highest for 15˚ and it decreases with increase in cover inclination. The average slope of the curves during increase in exergy destruction is lower in comparison to average slope during decrease in exergy destruction. The difference between maximum exergy destruction in east and west side, increases with increase in cover inclination. The average exergy destruction from water from east side was maximum in 15˚ still which was 11.94% higher than 30˚ still and 12.94% higher than 45˚ still whereas that on west side was also maximum in 15˚ still which was 14.07% higher than 30˚ still and 30.49% higher than 45˚ still.

Variation in exergy destruction from basin liner with time is represented in Figure 14. The maximum exergy destruction calculated from basin liner of east side of 15˚, 30˚ and 45˚ inclined distiller units was found to be highest in 45˚ distiller unit which was 1.66% and 2.31% higher than 30˚ and 15˚ units respectively. The maximum exergy destruction, evaluated from basin liner of west sides of 15˚, 30˚ and 45˚ inclined distiller units, was found to be highest in 45˚ inclined DSSS, which was marginally higher than 30˚ and 1.24% higher than 15˚ still. But maximum average exergy destruction, from basin liner of east side, was evaluated 406.77 W in 15˚ inclined distiller unit, which was 6.8% and 11.11% higher than 30˚ and 45˚ inclined units, whereas maximum average exergy destruction from basin liner of west side was evaluated 387.72 W, that too in 15˚ inclined distiller unit, which was 7.92% and 16.72% higher than 30˚ and 45˚ stills.

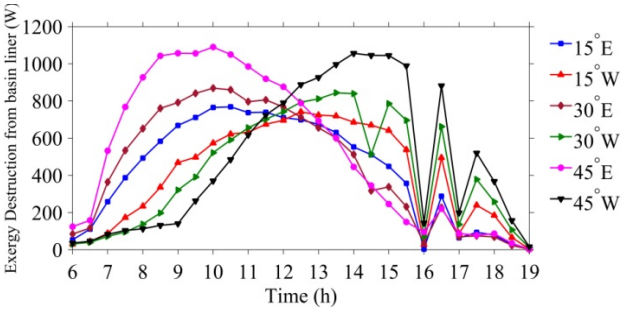


**Fig. 14. Variation in exergy destruction from basin liner with time.**

Exergy destruction has been evaluated from glass covers of east and west side of all the distiller units and its value with time is represented in Fig. 15. The exergy destruction from east side glass covers of all the distiller units is observed maximum, 56.97 W, in 30˚ distiller unit at 11:30 h, which is 2.64% and 7.88% higher than 15˚ and 45˚ distiller units respectively, while that from west side glass covers is observed maximum, 59.46 W, in 30˚ distiller unit, at 13:00 h, which is 2.3% and 1.22% higher than 15˚ and 45˚ distiller units respectively. But average exergy destruction, from eastern glass covers of all the distiller units, was calculated to have maximum value of 30.64 W, for 15˚ distiller unit, which is marginally (.008%) higher than 30˚ distiller unit, but 9.39% higher than 45˚ distiller unit, whereas from western covers of all the units, it was observed 30.09 W maximum, from 15˚ distiller unit, which is 3.97% and 8.31% higher than 30˚ and 45˚ distiller units, respectively. It has also been observed that the values of exergy destruction from basin liner are much higher in comparison to those from basin liner and glass covers.

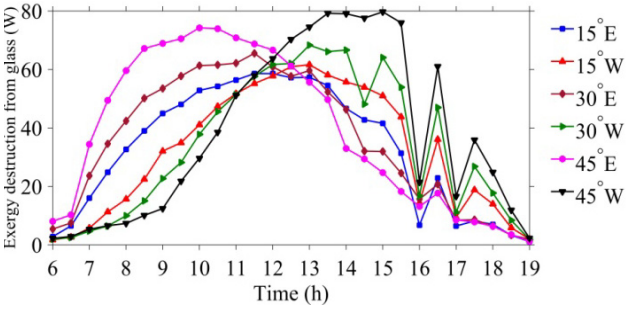


**Fig. 15. Variation in exergy destruction from glass with time**

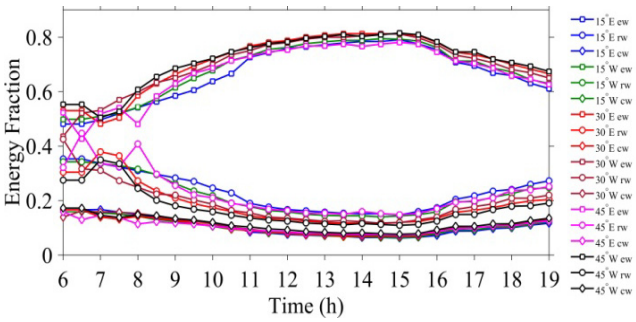


**Fig. 16. Variation of energy fractions with respect to time**

Three heat transfer modes i.e. evaporative, radiative and convective are responsible for vapour transport from water surface to condensing cover, thus produce distillate output. Their values have been calculated, using Kumar & Tiwari model, and from these values their contribution in the process has been evaluated. The contribution of each mode of heat transfer, as energy fraction is plotted with time in Fig. 16. It is clear from the graph that, the evaporative energy fraction, contributes most in the process followed by radiative and convective energy fraction. The evaporative energy fraction is minimum in the morning, it increases with time till noon (14:00 h), and then starts dropping, whereas radiative and convective energy fractions are higher in morning and evening and touch their minimum value in noon, from 12:00 h to 15:00 h.

The maximum evaporative energy fraction in east side in all the distiller units is evaluated and is observed maximum as 0.81 at 13:30 h in 30˚ still which is 2.53% and 3.84% higher than 15˚ and 45˚ distiller units respectively, whereas in west side, the maximum evaporative energy fraction is observed as 0.81 in 30˚ and 45˚ unit at 14:30 and 15:00 h respectively, which is 1.25% higher than 15˚. The minimum evaporative energy fraction in east side in all the stills is evaluated

and is observed lowest as 0.43 in at 6:30 h which is 10.4% and 8.5% lower than 15˚ and 30˚ still respec–tively, whereas minimum evaporative energy fraction in west side in all the distiller units is observed lowest 0.43 at 6:00 h in 30˚ unit which is 14% lower than 15˚ and 45˚ unit. The average evaporative energy fraction of east and west side, of individual distiller units has also been evaluated. On east side it is observed as 0.71 in 30˚ unit as maximum which is 5.97% higher than 15˚ and 45˚ distiller units, whereas on west side, it is observed maximum as 0.71 in 45˚ unit, and is 4.41% and 1.43% higher than 15˚ and 30˚ distiller units respectively. The maximum convective energy fraction for east side of all the distiller units, was evaluated and its highest value was observed as 0.17 at 6:00 h, in 15˚ unit, which is 6.25% higher than 30˚ and 45˚ distiller units respec–tively, whereas on the west side, it was observed to have maximum value 0.17 in 45˚ unit at 6:00 h, which is 6.25% higher than 15˚ and 30˚ distiller units respec–tively. The minimum convective energy fraction in west side of all the distiller units was found to have minimum value as 0.06 at 13:00 h in 15˚ unit, which is 14.29% and 25% lower than 30˚ and 45˚ distiller units respec–tively. However, the average convective energy fraction in east side of all the distiller units was eva–luated as 0.1, whereas in west side, it was evaluated as 0.11 in 30˚ and 45˚ distiller units which was 10% higher than 15˚ unit. The maximum radiative energy fraction, for east side of all the distiller units, was evaluated and it was found to be highest in 45˚ unit as 0.44 at 6:30 h, which is respectively 25.71% and 12.82% higher than 15˚ and 30˚ distiller units, whereas on the west side, it was found to have highest value as 0.43 at 6:00 h in 30˚ unit, which is 22.86% higher than 15˚ and 45˚ distiller units. The minimum radiative energy fraction, in east side of all the distiller units, was found to be lowest 0.12 in 30˚ unit, at 13:30 h, which was 20% lower than 15˚ and 45˚ distiller units, whereas on west side of all the units, it was found to have lowest value 0.11, at 15:00 h in 45˚ unit, which was 21.43% and 8.33% lower than 15˚ and 30˚ units respectively. The average radiative energy fraction, on eastern side of all the distiller units, was found to be 0.23 as maximum, in 15˚ unit, which was 21.05% and 4.5% higher, than 30˚ and 45˚ distiller units respectively, whereas on western side also it was maxi–mum as 0.22, in 15˚ unit, which was 15.79% higher than 30˚ unit and 29.41% higher than 45˚ unit.

The distillate output of the distiller units has been recorded, and used in Kumar & Tiwari model for evaluation of theoretical yield. Experimental and theo–retical distillate outputs, have been plotted in Fig. 17. with respect to time. Maximum distillate outputs, from the east side of 15˚, 30˚ and 45˚ distiller units, are recorded as 0.187, 0.167 and 0.146 kg/m$^2$-h at 14:00 h respectively whereas minimum is recorded 0.003 kg/m$^2$-h at 6:00 h respectively in all the three distiller units. Similarly maximum distillate output, from the west sides of 15˚, 30˚ and 45˚ distiller units are recorded as 0.174, 0.165 and 0.162 kg/m$^2$-h at 14:00 h respectively, whereas minimum was recorded as 0.003 kg/m$^2$-h at 6:00 h for all the three distiller units. The maximum yield recorded from east side of 15˚ unit was 12% and 28.1% higher than 30˚ and 45˚ distiller units respec–tively, where as maximum yield recorded from west side of 15˚ distiller units was 5.5% and 7.4% higher than 30˚ and 45˚ distiller units respectively. Cumulative distillate output, from 6:00 h to 19:00 h, from east side of 15˚ unit was 2.41 kg/m$^2$, which was 12.3% and 36.39% higher than 30˚ and 45˚ units respectively, whereas from west side of 15˚ unit, it was 2.25 kg/m$^2$, which was 4.7% higher than 30˚ unit and 2.6% higher than 45˚unit. In 15˚ inclined distiller unit, contribution of east and west sides were 52% and 48% respectively, whereas in 30˚ inclined distiller unit the contribution of both sides was equal and in 45˚ inclined distiller unit, the contribution from east and west side were 45% and 55% respectively. In 15˚ distiller unit, actual output was found 17.72% higher than predicted by Kumar &Tiwari model, whereas in 30˚ it was 12.58% lower than predicted and in 45˚ distiller unit, it was 14.14% lower than predicted.

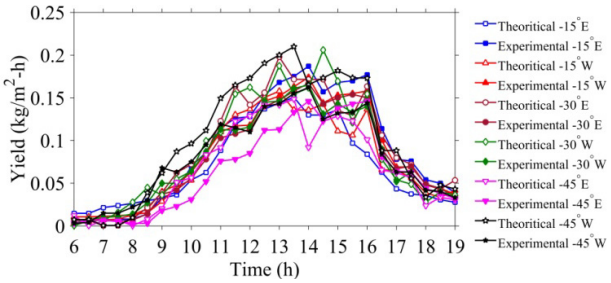


**Fig. 17. Theoretical and experimental yield from east and west sides of all the distiller units with time.**

## CONCLUSIONS

On the basis of experimental and theoretical results the following interesting conclusions are drawn:

- The distillate output of DSSS depends on the tempe–rature gradient between water & glass cover and glass & ambient temperature.
- Maximum distillate output has been recorded (4.66 l) in DSSS having 15˚inclined glass cover which is 8.52% and 17.7% higher as compared to 30˚ and 45˚ inclined glass cover DSSS respectively.
- Behaviour of east and west side of stills is very much identical for 30˚still but are quite different for 15˚ and 45˚stills.
- Average exergy destruction from basin liner is quite high in comparison to that from water and glass.

## REFERENCES

[1] Fathy M, Hassan H, Ahmed MS. Experimental study on the e ff ect of coupling parabolic trough collector with double slope solar still on its per–formance. Sol Energy 2018;163:54–61. doi:10.10 16/j.solener.2018.01.043.

[2] Saini V. et al.: Electrical and thermal energy assessment of series connected N partially covered photovoltaic thermal (PVT)-compound parabolic concentrator (CPC) collector for different solar cell materials. Appl Therm Eng 2018;128:1611–23. doi:10.1016/j.appl thermaleng.2017.09.119.

[3] Kalbasi R, Alemrajabi AA, Afrand M. Thermal modeling and analysis of single and double effect

solar stills: An experimental validation. Appl Therm Eng 2018;129. doi:10.1016/j.applthermal eng.2017.10.012.

[4] Kabeel AE, El-maghlany WM. Comparative study on the solar still performance utilizing different PCM. Desalination 2018;432:89–96. doi:10.1016 /j.desal.2018.01.016.

[5] Madhu B, Bala Subramanian E, Nagarajan PK, Sathyamurthy R, Mageshbabu D. Improving the yield of freshwater and exergy analysis of conven–tional solar still with different nanofluids. FME Trans 2017;45:524–30. doi:10.5937/fmet1704 524M.

[6] Sahota L, Tiwari GN. ScienceDirect Effect of $Al_2O_3$ nanoparticles on the performance of passive dou–ble slope solar still. Sol Energy 2016; 130:260–72. doi:10.1016/j.solener.2016.02.018.

[7] Moradi R, Kianifar A, Wongwises S. Optimization of a solar air heater with phase change materials: Experimental and numerical study. Exp Therm Fluid Sci 2017;89:41–9. doi:10.1016/j.expthermflu sci.2017.07.011.

[8] Rajaseenivasan T, Elango T, Kalidasa Murugavel K. Comparative study of double basin and single basin solar stills. Desalination 2013;309:27–31. doi:10.1016/j.desal.2012.09.014.

[9] Tiwari AK, Tiwari GN. Thermal modeling based on solar fraction and experimental study of the annual and seasonal performance of a single slope passive solar still: The effect of water depths. Desalination 2007;207:184–204. doi:10.1016/j. desal.2006.07.011.

[10] Elango C, Gunasekaran N, Sampathkumar K. Thermal models of solar still-A comprehensive review. Renew Sustain Energy Rev 2015;47:856–911. doi:10.1016/j.rser.2015.03.054.

[11] Mishra DR, Tiwari AK. Effect of coal and metal chip on the solar still. J Sci Tech Res 2013;3:1–6.

[12] Hidouri K. et al. Experimental Evaluation of Influ–ence of Air Injection Rate on a Novel Single Slope Solar Still Integrated with an Air Compre–ssor. Glob J Res Eng A Mech Mech Eng 2017; 17:30–9.

[13] Hidouri K, Mishra DR, Benhmidene A, Chouachi B. Experimental and theoretical evaluation of a hybrid solar still integrated with an air compressor using ANN. Desalin WATER Treat 2017;88:52–9. doi:10.5004/dwt.2017.21333.

[14] Dumka P, Mishra DR. Energy and exergy analysis of conventional and modified solar still integrated with sand bed earth: Study of heat and mass tran–sfer. Desalination 2018;437:15–25. doi:10.1016 /j. desal.2018.02.026.

[15] Dumka P,. et al. Experimental investigation of modi–fied single slope solar still integrated with earth (I) & (II): Energy and exergy analysis. Energy 2018; 160: 1144–57. doi:DOI: 10.1016/j.energy. 2018.07. 083.

[16] Akash BA, Mohsen MS, Nayfeh W. Experimental study of the basin type solar still under local cli–mate conditions. Energy Convers Manag 2000; 41: 883–90. doi:10.1016/S0196-8904(99) 00158-2.

[17] Murugavel KK, Srithar K, Kalidasa Murugavel K, Srithar K. Performance study on basin type double slope solar still with different wick materials and minimum mass of water. Renew Energy 2011 ;36:612–20. doi:10.1016/j.renene.2010.08.009.

[18] Dwivedi VK, Tiwari GN. Comparison of internal heat transfer coefficients in passive solar stills by different thermal models: An experimental valida–tion. Desalination 2009;246:304–18. doi:10.1016/j. desal.2008.06.024.

[19] Elango T, et al. The effect of the water depth on the productivity for single and double basin double slope glass solar stills. Desalination 2015;359:82–91. doi:10.1016/j.desal. 2014.12.036.

[20] Srithar K. et al. Performance analysis on a solar bubble column humidification dehumi–dification desalination system. Process Saf Environ Prot 2017;105:41–50. doi:10.1016/j.psep. 2016.10. 002.

[21] Panchal HN, Shah PK. Effect of varying glass cover thickness on performance of solar still: In a winter climate conditions. Int J Renew Energy Res 2011;1:212–23.

[22] Hung TC. et al. Numerical analysis and experi–mental validation of heat transfer characteristic for flat-plate solar air collector. Appl Therm Eng 2017; 111: 1025–38. doi:10.1016/j.applthermaleng.2016. 09.126.

[23] Sharma M, Tiwari AK, Mishra DR. A review on desalination of water using single slope passive solar still. Int J Dev Res 2016;06:10002–12.

[24] Leśny J, Panfil M, Urbaniak M. Influence of irra–diance and irradiation on characteristic para–meters for a solar air collector prototype. Sol Energy 2018; 164:224–30. doi:10.1016/j.solener.2018.02. 047.

[25] Agrawal S, Tiwari GN. Energy and exergy analysis of hybrid micro-channel photovoltaic thermal mo–dule. Sol Energy 2011;85:356–70. doi:10.1016/ j.solener.2010.11.013.

[26] Toyama S, Aragak T, Salah HM, Murase K, Sando M. Simulation of a Multieffect Solar Still and the Static Characteristics. J Chem Eng Japan 1987; 20:473–8. doi:10.1252/jcej.20.473.

[27] [27] Dunkle RV. Solar Water Desalination: The Roof Type Still and a Multiple Effect Diffusion Still. Int. Dev. Heat Transf., 1961, p. 895–902.

[28] Clark JA. The steady-state performance of a solar still. Sol Energy 1990;44:43–9. doi:10.1016/0038-092X(90)90025-8.

[29] Kumar S, Tiwari GN. Estimation of convective mass transfer in solar distillation systems. Sol Ene–rgy 1996;57:459–64. doi:10.1016/S0038-092X (96) 00122-3.

[30] Tiwari GN, Tiwari AK. Solar Distillation Practice for Water Desalination Systems. New Delhi, India: Anamaya; 2008.

[31] Malik MAS et al. Solar distillation. Oxford, UK: Pergamon Press; 1982.

[32] Petela R. Exergy of Heat Radiation. J Heat Transfer 1964;86:187. doi:10.1115/1.3687092.

[33] Petela R. Exergy of undiluted thermal radiation. Sol Energy 2003;74:469–88. doi:10.1016/S0038-092X (03)00226-3.

## ЕКСПЕРИМЕНТАЛНА И ТЕОРИЈСКА ЕВАЛУАЦИЈА СОЛАРНИХ ДЕСТИЛАТОРА СА ЈЕДНИМ БАЗЕНОМ ПОД ДВОСТРУКИМ НАГИБОМ: АНАЛИЗА ПРЕНОСА ТОПЛОТЕ И МАСЕ

**М. Дубеј, Д.Р. Мишра**

Извршена је теоријска и експериментална анализа три соларна дестилатора са по једним базеном под двоструким нагибом стакленог колектора: $15^0$, $30^0$ и $45^0$ у метеоролошким условима Рагогара, Гуна ($24^0$39' сев. геогр. ширине и $77^0$19'ист. геогр. дужине, Индија). Експерименти су извођени од 14-16. јуна 2017. Детаљна анализа енергије и ексергије извршена је помоћу теоријског модела Кумара и Тиварија бази–раног на регресионој анализи.

Теоријски резултати добијени евалуацијом слажу се са експерименталним резултатима. Максимална коли–чина слатке воде је добијена под нагибом стакленог колектора од $15^0$ (кол. воде 4,66 л у 14:00 часова) и учешћем соларног дестилатора од 52% односно 48% на источној односно западној страни. У 15:00 часова сви дестилатори су показали максималну термичку ефикасност, тј. 23,69; 29,24 и 25,09% при нагибу колектора од $15^0$, $30^0$ и $45^0$. Утврђено је да се максимална ексергија јавља у базену са стаклом и водом код свих соларних дестилатора са двоструким нагибом.